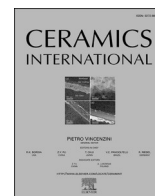




Contents lists available at ScienceDirect

Ceramics International

journal homepage: [www.elsevier.com/locate/ceramint](http://www.elsevier.com/locate/ceramint)

## Expanding gaufreyite family to $\text{Sr}_2\text{MBi}(\text{REEO})_3(\text{BO}_3)_4$ ( $M = \text{Ca}, \text{Sr}, \text{Ba}$ ; $\text{REE} = \text{Y}, \text{Eu}$ ) borates with large second harmonic generation responses

R.S. Bubnova<sup>a,b,\*</sup>, A.P. Shablinskii<sup>a</sup>, S. Yu Stefanovich<sup>c</sup>, M. Yu Arsent'ev<sup>a</sup>,  
M.G. Krzhizhanovskaya<sup>a,b</sup>, B.I. Lazoryak<sup>c</sup>, V.L. Ugolkov<sup>a</sup>, S.K. Filatov<sup>b</sup>

<sup>a</sup> Institute of Silicate Chemistry of the Russian Academy of Sciences ISC RAS, Makarova Emb. 2, Saint Petersburg, 199034, Russia

<sup>b</sup> Institute of Earth Sciences, Saint Petersburg State University, Universitetskaya Emb. 7/9, Saint Petersburg, 199034, Russia

<sup>c</sup> Chemistry Department, Moscow State University, Leninskie Gory 1-3, Moscow, 119991, Russia

### ARTICLE INFO

Handling Editor: Dr P. Vincenzini

#### Keywords:

Nonlinear optical materials  
Second harmonic generation  
Borates  
Thermal expansion  
Crystal structure  
Electronic structure

### ABSTRACT

The synthesis, crystal structure, and characterization of a few new noncentrosymmetric rare-earth borates of gaufreyite family  $\text{Sr}_2\text{MBi}(\text{REEO})_3(\text{BO}_3)_4$  ( $M = \text{Ca}, \text{Sr}, \text{Ba}$ ;  $\text{REE} = \text{Y}, \text{Eu}$ ) are represented. Samples of  $\text{Sr}_2\text{MBi}(\text{YO})_3(\text{BO}_3)_4$  ( $M = \text{Ca}, \text{Sr}, \text{Ba}$ ) borates were synthesized by multi-step solid state reactions. The crystal structures of  $\text{Sr}_3\text{Bi}(\text{YO})_3(\text{BO}_3)_4$ ,  $\text{Sr}_2\text{CaBi}(\text{YO})_3(\text{BO}_3)_4$  and  $\text{Sr}_2\text{BaBi}(\text{YO})_3(\text{BO}_3)_4$  were refined in  $P6_3$  space group to  $R_1$  0.059, 0.058 and 0.018, respectively. Second-harmonic generation measured with Kurtz-Perry powder technique shows an increase in the nonlinear optical activity of materials by almost two times upon partial substitutions of Sr for Ca and Ba in the  $\text{Sr}_3\text{Bi}(\text{REEO})_3(\text{BO}_3)_4$  and its decrease if Y atoms are replaced by Eu. Thermal expansion coefficients for  $\text{Sr}_2\text{MBi}(\text{YO})_3(\text{BO}_3)_4$  ( $M = \text{Ca}, \text{Sr}, \text{Ba}$ ) borates and  $\text{Ca}_4(\text{MnO})_3(\text{BO}_3)_3(\text{CO}_3)$  gaufreyite are calculated for the first time. Thermal expansion of these compounds is almost isotropic due to the arrangement of  $\text{BO}_3$  units which are located in the  $ab$  and  $ac$  planes.

### 1. Introduction

In the recent decades, crystal structures with planar anionic groups [ $\text{TO}_3$ ] have been of great interest among nonlinear optical (NLO) materials. Influence of [ $\text{BO}_3$ ]<sup>3-</sup>, [ $\text{CO}_3$ ]<sup>3-</sup>, [ $\text{NO}_3$ ]<sup>-</sup>, [ $\text{B}_3\text{O}_6$ ]<sup>3-</sup> anionic groups on NLO properties are reviewed in Refs. [1–3]. Compounds containing these groups have large second harmonic generation (SHG) and birefringence characteristics, making these compounds promising candidates for achieving high conversion efficiency for NLO applications. Most materials containing [ $\text{BO}_3$ ] and [ $\text{CO}_3$ ] groups are transparent from visible to deep-ultraviolet regions [1]. Owing to the configuration, the [ $\text{BO}_3$ ] groups will exhibit a large optical anisotropy between the two directions, which is parallel and perpendicular to the plane of triangles [4]. Typically, planes of [ $\text{BO}_3$ ] triangles are parallel or practically parallel to each other. That arrangement of planar triangular groups leads to high anisotropy of thermal expansion [5].

After discovery of  $\alpha$ - $\text{BiB}_3\text{O}_6$  famous NLO-borate [6], special attention was focused on the search for other non-centrosymmetric Bi-containing borates. As well NLO materials based on rare earth elements keep attracting broad interest because the highly distorted structural motifs

centered by rare earth ions could remarkably benefit the second harmonic generation [7].

There is (Bi, REE)-containing borate,  $\text{Sr}_3\text{Bi}(\text{YO})_3(\text{BO}_3)_4$  [8], with moderate SHG response related to gaufreyite  $\text{Ca}_4(\text{MnO})_3(\text{BO}_3)_3(\text{CO}_3)$  [9,10]. Among the members of gaufreyite family only  $\text{Sr}_3\text{Bi}(\text{YO})_3(\text{BO}_3)_4$  and  $\text{Cd}_3\text{Bi}(\text{AlO})_3(\text{BO}_3)_4$  [11] are crystallized in non-centrosymmetric space group  $P6_3$  while others –  $\text{Ca}_3\text{Y}(\text{MnO})_3(\text{BO}_3)_4$  [12],  $\text{Ca}_3\text{Y}(\text{AlO})_3(\text{BO}_3)_4$ ,  $\text{Ca}_3\text{Y}(\text{GaO})_3(\text{BO}_3)_4$  [13],  $\text{Ca}_3\text{Y}(\text{VO}_3)(\text{BO}_3)_4$  [14] are centrosymmetric and crystallized in  $P6_3/m$  space group. Borates of gaufreyite-type are studied as magnetic materials with a kagome lattice (e.g.  $\text{Ca}_3\text{Y}(\text{VO}_3)(\text{BO}_3)_4$ ) [14]. In the gaufreyite structure type, there are  $\text{BO}_3$  groups are arranged perpendicular to each other or close to these directions.

Promising NLO properties of gaufreyite-type  $\text{Sr}_3\text{Bi}(\text{YO})_3(\text{BO}_3)_4$  [8,14–16] stimulated further investigations of borates in this family. In particular, it was shown that asymmetric Bi coordination polyhedra and arrangement of borate groups give the main contributions to the NLO properties in the Bi-containing borates. These contributions strongly depend on crystal structure details, chemical nature of cations, and distribution of cations over sites in crystal structure [4,17]. Cation

\* Corresponding author. Institute of Silicate Chemistry of the Russian Academy of Sciences ISC RAS, Makarova Emb. 2, Saint Petersburg, 199034, Russia.

E-mail address: [rimma\\_bubnova@mail.ru](mailto:rimma_bubnova@mail.ru) (R.S. Bubnova).

<https://doi.org/10.1016/j.ceramint.2023.01.091>

Received 19 October 2022; Received in revised form 23 December 2022; Accepted 11 January 2023

Available online 13 January 2023

0272-8842/© 2023 Published by Elsevier Ltd.

**Table 1**  
Crystal data, data collection information and structure refinement details.

Chemical formula	Sr <sub>2</sub> CaBi (YO) <sub>3</sub> (BO <sub>3</sub> ) <sub>4</sub>	Sr <sub>2</sub> Bi (YO) <sub>3</sub> (BO <sub>3</sub> ) <sub>4</sub>	Sr <sub>1.80</sub> Ba <sub>1.20</sub> Bi (YO) <sub>3</sub> (BO <sub>3</sub> ) <sub>4</sub> <sup>a</sup>
<i>M<sub>r</sub></i>	974.2	1008.9	1081.5
Crystal system, sp. gr.	Hexagonal, <i>P</i> 6 <sub>3</sub>		
Temperature (K)	293		
<i>a</i> , <i>c</i> (Å)	10.624 (1), 6.6591 (7)	10.730 (2), 6.726 (1)	10.78028 (8), 6.74379 (6)
<i>V</i> (Å <sup>3</sup> )	650.9 (1)	670.7 (2)	678.73(1)
<i>Z</i>	2		
Radiation type	Mo <i>K</i> α		Cu <i>K</i> α
<i>μ</i> (mm <sup>-1</sup> )	35.31	36.90	76.30
Crystal size (mm)	0.2 × 0.2 × 0.07	0.1 × 0.2 × 0.04	–
Data collection			
Diffractometer	Bruker Smart APEX II		Rigaku Ultima IV
Absorption correction	Multi-scan		
No. of measured, independent and observed [ <i>I</i> > 3σ( <i>I</i> )] reflections	6623, 712, 639	6652, 659, 653	–
(sin <i>θ</i> / <i>λ</i> ) <sub>max</sub> (Å <sup>-1</sup> )	0.711	0.707	0.562
Refinement			
<i>R</i> [ <i>F</i> <sup>2</sup> > 2σ( <i>F</i> <sup>2</sup> )], <i>wR</i> ( <i>F</i> <sup>2</sup> ), <i>S</i>	0.059, 0.054, 1.80	0.058, 0.061, 2.18	0.018, 7.35, 2.73
No. of reflections	712	659	375
No. of ref. parameters	48	69	43
Absolute structure	297 of Friedel pairs used in the refinement	287 of Friedel pairs used in the refinement	–

<sup>a</sup> The Rietveld refinement data.

substitutions can lead to multifunctional materials with a combination of properties such as high non-linear optical activity due to structural distortions caused by the presence of different cations in the same sites. The inclusion of activator ions (e.g. Eu<sup>3+</sup>) in the composition of NLO crystals can lead to the preparation of self-frequency-doubling crystals (e.g. Ref. [18]).

In the present work, we choose the Sr<sub>3</sub>Bi(YO)<sub>3</sub>(BO<sub>3</sub>)<sub>4</sub> NLO borate as a starting point for replacing Sr with Ca and Ba, and also Y with Eu, in order to investigate influence of cation substitutions on NLO properties and to expand the gaudfroyite family with new members Sr<sub>2</sub>MBi(YO)<sub>3</sub>(BO<sub>3</sub>)<sub>4</sub> (*M* = Ca, Ba) and Sr<sub>2</sub>BaBi(EuO)<sub>3</sub>(BO<sub>3</sub>)<sub>4</sub>. Here we report the synthesis of these borates using solid state reactions and their structural characterization with powder and single-crystal X-ray diffraction as well as studies of their NLO and thermal properties.

## 2. Experimental

### 2.1. Synthesis

The powder samples of Sr<sub>2</sub>MBi(YO)<sub>3</sub>(BO<sub>3</sub>)<sub>4</sub> (*M* = Ca, Sr, Ba) and Sr<sub>2</sub>BaBi(EuO)<sub>3</sub>(BO<sub>3</sub>)<sub>4</sub> borates were synthesized by multi-step solid state reactions. Initial reagents SrCO<sub>3</sub>, BaCO<sub>3</sub>, CaCO<sub>3</sub>, Bi<sub>2</sub>O<sub>3</sub>, H<sub>3</sub>BO<sub>3</sub>, Y<sub>2</sub>O<sub>3</sub>, Eu<sub>2</sub>O<sub>3</sub> (99.99% purity) were mixed in stoichiometric ratios. This mixture was ground into pellets and placed in platinum crucibles. The pellets were heated at 300 °C for 5 h and at 500 °C for 5 h. Then the pellets were heated at 950 °C for 24 h. The pellets were then reground, pressed into pellets again and finally heated at 1000 °C for 40 h.

Single crystals of title compounds were prepared by additional heat-treatment of the tablets varying the temperature around the decomposition temperature (1100 ± 30) °C for 28 h. The temperature in the furnace was maintained in the range of 1070–1100 °C, at which the Sr<sub>2</sub>MBi(YO)<sub>3</sub>(BO<sub>3</sub>)<sub>4</sub> borates have to decompose on heating and then crystallize again upon slight cooling. Solid-state phase transformations proceed slowly and the crystals do not have time to completely decompose. The crystals begin to recrystallize again and can reach sizes suitable for single crystal X-ray diffraction. Then, the samples were

**Table 2**  
Selected bond lengths (Å).

Bond	Distance, Å	<i>BV</i>	Bond	Distance, Å	<i>BV</i>
Sr <sub>2</sub> CaBi(YO) <sub>3</sub> (BO <sub>3</sub> ) <sub>4</sub>					
Bi1–O5	2.02(2)	0.94	Sr1–O3	2.41(2)	0.40
Bi1–O5	2.02(3)	0.94	Sr1–O2	2.52(3)	0.29
Bi1–O5	2.02(2)	0.94	Sr1–O3	2.57(2)	0.26
Bi1–O4	2.93(2)	0.10	Sr1–O5	2.60(2)	0.24
Bi1–O4	2.93(2)	0.10	Sr1–O3	2.63(2)	0.22
Bi1–O4	2.93(3)	0.10	Sr1–O1	2.63(2)	0.22
<Bi1–O> <sub>6</sub>	2.51		Sr1–O4	2.63(2)	0.22
Y1–O1	2.27(2)	0.51	Sr1–O4	2.76(2)	0.15
Y1–O5	2.24(2)	0.55	<Sr1–O> <sub>8</sub>	2.59	2.00
Y1–O1	2.33(2)	0.43	B2–O1	1.37(3)	1.00
Y1–O5	2.47(3)	0.30	B2–O4	1.39(4)	0.95
Y1–O4	2.40(2)	0.36	B2–O2	1.40(4)	0.92
Y1–O2	2.28(2)	0.49	<B2–O> <sub>3</sub>	1.39	2.87
Y1–O2	2.53(2)	0.24	O5–Bi1	2.02(2)	0.94
<Y1–O> <sub>7</sub>	2.36	2.87	O5–Y1	2.24(2)	0.55
B1–O3	1.37(2)	1.00	O5–Y1	2.47(3)	0.30
B1–O3	1.37(2)	1.00	O5–Sr1	2.60(2)	0.24
B1–O3	1.37(3)	1.00	<O <sub>ex</sub> –M> <sub>4</sub>	2.33	2.03
<B1–O> <sub>3</sub>	1.37	3.00			
Sr <sub>3</sub> Bi(YO) <sub>3</sub> (BO <sub>3</sub> ) <sub>4</sub>					
Bi1–O5	2.07(4)	0.85	Sr1–O3	2.50(2)	0.36
Bi1–O5	2.07(4)	0.85	Sr1–O2	2.59(3)	0.28
Bi1–O5	2.07(4)	0.85	Sr1–O3	2.51(2)	0.35
Bi1–O4	2.97(3)	0.09	Sr1–O3	2.60(2)	0.27
Bi1–O4	2.97(3)	0.09	Sr1–O5	2.67(2)	0.22
Bi1–O4	2.97(4)	0.09	Sr1–O1	2.70(3)	0.21
<Bi1–O> <sub>6</sub>	2.52	2.82	Sr1–O4	2.76(2)	0.18
Y1–O1	2.27(2)	0.51	Sr1–O4	2.79(2)	0.16
Y1–O5	2.31(3)	0.45	<Sr1–O> <sub>8</sub>	2.64	2.03
Y1–O1	2.39(4)	0.37	B2–O1	1.39(6)	0.95
Y1–O5	2.31(3)	0.45	B2–O4	1.41(6)	0.90
Y1–O4	2.35(2)	0.41	B2–O2	1.42(7)	0.88
Y1–O2	2.42(2)	0.34	<B2–O> <sub>3</sub>	1.41	2.73
Y1–O2	2.42(2)	0.34	O5–Bi1	2.07(4)	0.85
<Y1–O> <sub>7</sub>	2.35	2.85	O5–Y1	2.31(3)	0.45
B1–O3	1.40(2)	0.92	O5–Y1	2.31(3)	0.45
B1–O3	1.40(2)	0.92	O5–Sr1	2.67(2)	0.22
B1–O3	1.40(4)	0.92	<O <sub>ex</sub> –M> <sub>4</sub>	2.34	1.97
<B1–O> <sub>3</sub>	1.40	2.77			
Sr <sub>2</sub> BaBi(YO) <sub>3</sub> (BO <sub>3</sub> ) <sub>4</sub>					
Bi1–O5	2.09 (2)	0.81	Sr1–O3	2.35(2)	0.53
Bi1–O5	2.09 (2)	0.81	Sr1–O2	2.62(2)	0.26
Bi1–O5	2.09 (2)	0.81	Sr1–O3	2.69(2)	0.21
Bi1–O4	3.03 (3)	0.08	Sr1–O3	2.70(1)	0.21
Bi1–O4	3.03 (3)	0.08	Sr1–O5	2.70(2)	0.21
Bi1–O4	3.03 (3)	0.08	Sr1–O1	2.70(2)	0.17
<Bi1–O> <sub>6</sub>	2.56	2.68	Sr1–O4	2.77(2)	0.16
Y1–O1	2.15(2)	0.70	Sr1–O4	2.80(3)	0.21
Y1–O5	2.29(2)	0.44	<Sr1–O> <sub>8</sub>	2.66	1.96
Y1–O1	2.32(2)	0.36	B2–O1	1.39(5)	0.95
Y1–O5	2.35(2)	0.29	B2–O4	1.34(4)	1.08
Y1–O4	2.40(2)	0.27	B2–O2	1.41(5)	0.90
Y1–O2	2.48(2)	0.47	<B2–O> <sub>3</sub>	1.38	2.93
Y1–O2	2.50(2)	0.40	O5–Bi1	2.09 (2)	0.81
<Y1–O> <sub>7</sub>	2.36	2.93	O5–Y1	2.29(2)	0.44
B1–O3	1.38(2)	0.97	O5–Y1	2.35(2)	0.29
B1–O3	1.38(2)	0.97	O5–Sr1	2.70(2)	0.21
B1–O3	1.38(4)	0.97	<O <sub>ex</sub> –M> <sub>4</sub>	2.36	1.75
<B1–O> <sub>3</sub>	1.38	2.92			

removed from the muffle furnace and cooled in air. The samples were heterogeneous (Sr<sub>2</sub>MBi(YO)<sub>3</sub>(BO<sub>3</sub>)<sub>4</sub>, (Sr,*M*)<sub>3</sub>Y<sub>2</sub>(BO<sub>3</sub>)<sub>4</sub> and YBiO<sub>3</sub>), and the color changed from white to light-brown. Single crystals were selected from the pellets for the further single crystal X-ray diffraction experiment.

### 2.2. Powder X-ray diffraction

The powders were checked using a Rigaku MiniFlex II powder X-ray diffractometer with CuKα radiation, Bragg-Brentano geometry and PSD DTEX/ULTRA detector. The samples were prepared from the heptane

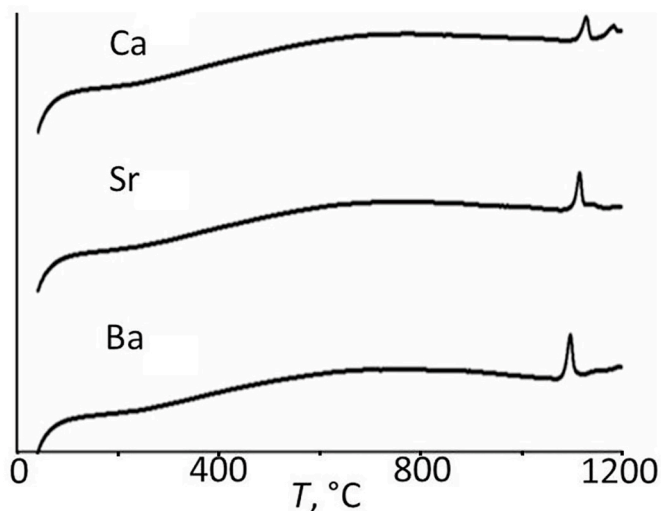


Fig. 1. DSC curves for  $\text{Sr}_2\text{MBi}(\text{YO})_3(\text{BO}_4)_4$  ( $M = \text{Ca}, \text{Sr}, \text{Ba}$ ) samples.

suspension. Unit cell parameters and unit cell volume as well as phase composition were refined by the least squares method. Phase identification shows that the resulting samples are homogeneous and isotypical although  $\text{Sr}_2\text{BaBi}(\text{YO})_3(\text{BO}_3)_4$  sample contained about 3 wt % impurity of  $\text{Y}_2\text{O}_3$ . Powder diffraction data for the Rietveld refinement of  $\text{Sr}_2\text{BaBi}(\text{YO})_3(\text{BO}_3)_4$  were collected using a Rigaku Ultima IV diffractometer ( $\text{CuK}\alpha_{1+2}$ , 40 kV and 35 mA, Bragg-Brentano geometry, PSD DTEX/ULTRA detector,  $2\theta = 5\text{--}120^\circ$ , step  $0.02^\circ$ , exposure at point 5 s). Experimental data processing by the Rietveld refinement such as the refinement of zero shift, background approximation, peak shape parameters, unit cell parameters, atomic coordinates, isotropic displacement parameters and site occupancies were performed using Topas 5.0 [19] software (Tables 1 and 2; S1). The unit-cell parameters of  $\text{Sr}_2\text{Ba}(\text{EuO})_3(\text{BO}_3)_4$  obtained from powder X-ray diffraction data are  $a = 10.919$  (5),  $c = 6.752$  (4) Å,  $V = 697.2$  (6) Å<sup>3</sup>.

### 2.3. Single crystal X-ray diffraction

Single crystal X-ray diffraction data were collected using a Bruker Smart APEX II diffractometer using  $\text{MoK}\alpha$  radiation. The data were corrected for Lorentz, polarization and background effects using Bruker program APEX. A semi-empirical absorption-correction based on the intensities of equivalent reflections was applied in the SADABS program. The crystal structures of the  $\text{Sr}_2\text{MBi}(\text{YO})_3(\text{BO}_4)_4$  ( $M = \text{Ca}, \text{Sr}$ ) were solved by charge flipping and refined using Jana 2006 program suite [20] (Table 1). Atomic coordinates, atomic anisotropic displacement parameters and selected bond lengths are given in Tables S1–S2 and Table 2. Further details of the crystal structure investigations can be obtained from the Cambridge Structural Database on quoting the depository numbers CSD 2206303 and 2,206,306.

### 2.4. High temperature powder X-ray diffraction

High temperature powder X-ray diffraction study of  $\text{Sr}_2\text{MBi}(\text{YO})_3(\text{BO}_4)_4$  ( $M = \text{Ca}, \text{Sr}, \text{Ba}$ ) was performed using Rigaku Ultima IV powder diffractometer ( $\text{CoK}\alpha$  radiation,  $2\theta = 10\text{--}75^\circ$ , step  $0.02^\circ$ ) with high temperature chamber SHT-1500. The temperature was checked using  $\text{K}_2\text{SO}_4$  phase transition. The error in the determination of the temperature did not exceed  $10^\circ\text{C}$ . Temperature step was  $20^\circ\text{C}$  within range  $25\text{--}1100^\circ\text{C}$ . Average heating rate was about  $40^\circ\text{C}/\text{h}$ . The average heating rate was calculated taking into account the heating time between measurements, the temperature stabilization time before measurement (30 s), and the X-ray diffraction measurement time at each temperature. The temperature dependencies of unit cell parameters

were approximated by the second order polynomial function (Table S3). Unit cell parameters were refined at different temperatures by the Rietveld method using RietveldToTensor software [21], temperature dependences of unit-cell parameters and volume of borates were described by polynomial function. Based on the coefficients of approximation, the components of the tensor were calculated and the surface of the second-rank symmetric tensor – the figure of thermal expansion coefficients can be plotted using RTT software.

### 2.5. Thermal analysis

Differential scanning calorimetry and thermal gravimetric analysis (DSC + TG) were carried out using a STA 429 CD NETZSCH simultaneous thermal analysis instrument equipped with a platinum-rhodium sample holder (dynamic air atmosphere, air flow  $50\text{ cm}^3/\text{min}$ , temperature range  $40\text{--}1400^\circ\text{C}$ , heating rate  $20^\circ\text{C}/\text{min}$ ). Before the experiment, the calibration of a thermobalance was performed using  $\text{CaC}_2\text{O}_4 \times 2\text{H}_2\text{O}$  external standard. The accuracy of determination of the weight was  $\pm 0.01\text{ mg}$ . The temperature ( $^\circ\text{C}$ ) and sensitivity ( $\mu\text{V}/\text{mW}$ ) calibration of the Type S thermocouple was performed using In, Sn, Bi, Zn, Al, Au and Pb external standards. The errors in determinations of the temperature and sensitivity did not exceed  $\pm 2^\circ\text{C}$  and  $\pm 2$  relative percent, respectively. The pellet for the experiment was weighed with an accuracy of  $0.01\text{ mg}$  (the mass was approximately 17 mg) and placed in an open platinum-rhodium crucible. The temperatures of thermal effects were determined using a NETZSCH Proteus software by the DSC first derivative curve.

### 2.6. Second harmonic generation measurements

The second-harmonic generation (SHG) signals were measured using the Kurtz-Perry powder technique [22]. A Minilite-I Nd:YAG laser, operated in Q-switched mode with a repetition rate of 10 Hz, was the source of radiation at  $\lambda_{00} = 1064\text{ nm}$ . The radiation was directed onto the powder in order to produce the doubled frequency response of the second harmonics,  $\lambda_{200} = 532\text{ nm}$ . Green light of the second harmonic was collected in reflection mode and detected by a photomultiplier tube. In order to detect only light at 532 nm, a narrow band-pass interference filter was attached to the tube. Fig. S2 shows particle size distributions of  $\text{Sr}_3\text{Bi}(\text{YO})_3(\text{BO}_3)_4$ . The signal from the multiplier was measured with a digital lock-in amplifier and then registered by PC to be compared with that of  $\alpha\text{-SiO}_2$  powder standard sample with grain size of 3–5 mm.

### 2.7. Computational details

The calculations of  $\text{Sr}_3\text{Bi}(\text{YO})_3(\text{BO}_3)_4$  and  $\text{Sr}_2\text{CaBi}(\text{YO})_3(\text{BO}_3)_4$  were performed within the framework of the density-functional theory (DFT) as implemented in the SIESTA 4.0 program package [23]. The exchange-correlation potential within the Generalized Gradient Approximation (GGA) with the Perdew-Burke-Ernzerhof parametrization was used [24]. The core electrons were treated within the frozen core approximation, applying norm-conserving Troullier–Martins pseudopotentials [25] generated using ATOM 3.2.2. Program [23]. A real-space mesh cutoff of 350 Ry and the threshold of  $10^{-3}\text{ eV}$  were set for the self-consistent field convergence of the total electronic energy. In these atoms, Bi:  $6s^2 6p^3$ , Sr:  $5s^2$ , Y:  $5s^2 4d^1$ , B:  $2s^2 2p^1$ , O:  $2s^2 2p^4$  and Ca:  $4s^2$  were treated as valence electrons. The integration of the Brillouin zone was performed by a  $5 \times 5 \times 7$  k-point grid sampling for density of states of  $\text{Sr}_3\text{Bi}(\text{YO})_3(\text{BO}_3)_4$  and  $\text{Sr}_2\text{CaBi}(\text{YO})_3(\text{BO}_3)_4$ , and the Fermi level ( $E_f = 0\text{ eV}$ ) was selected as the reference.

For calculations of  $\text{Sr}_2\text{CaBi}(\text{YO})_3(\text{BO}_3)_4$ , we used a constructed set of elementary cells containing 52 atoms. Strontium and calcium atoms were distributed in various combinations in a ratio of 2 to 1. After that, the total energy was calculated for all combinations. As a result, the combination of calculations for which is shown (cf. Fig. 8) had the lowest total energy.

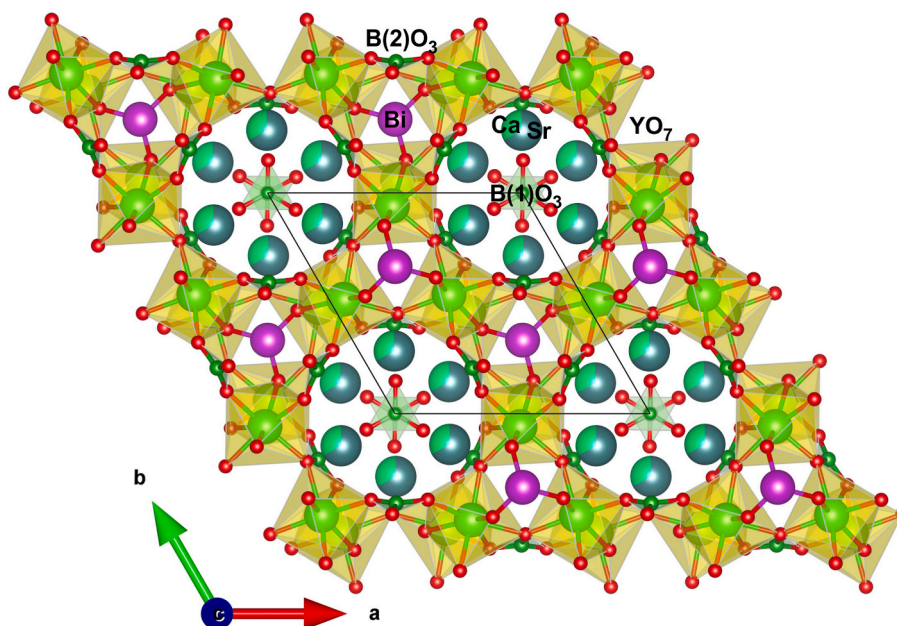


Fig. 2. Crystal structure of  $\text{Sr}_2\text{CaBi}(\text{YO})_3(\text{BO}_3)_4$ .

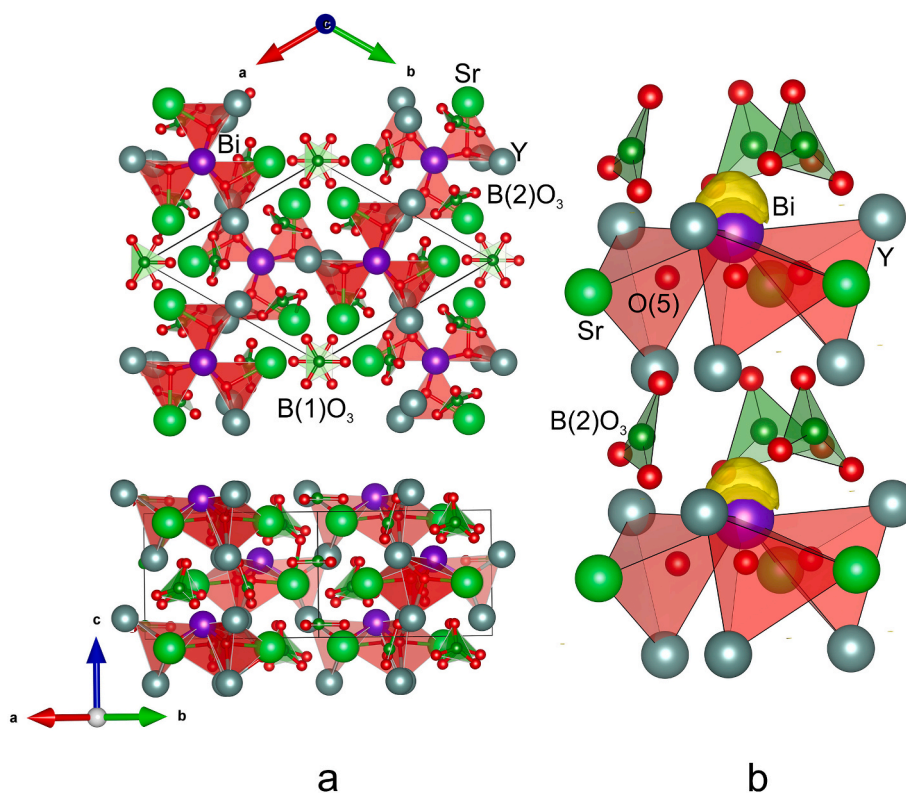


Fig. 3. Crystal structure of  $\text{Sr}_2\text{CaBi}(\text{YO})_3(\text{BO}_3)_4$  in terms of oxy-centered polyhedra (a); the ELF = 0.88 isosurface, which clearly identifies the lone electron pairs near the Bi atoms (b).

The calculated electron-density distribution was also analyzed using the electron localization function (ELF). The calculations were performed within the density functional theory (DFT) using a plane-wave basis set, as implemented in the Quantum ESPRESSO ab initio simulation package [26] (Version 5.4.0; Giannozzi et al., 2009). The Perdew–Burke–Ernzerhofs version of generalized gradient approximation was used for the description of the exchange–correlation functional. A cut-off energy was 640 eV.

### 3. Results

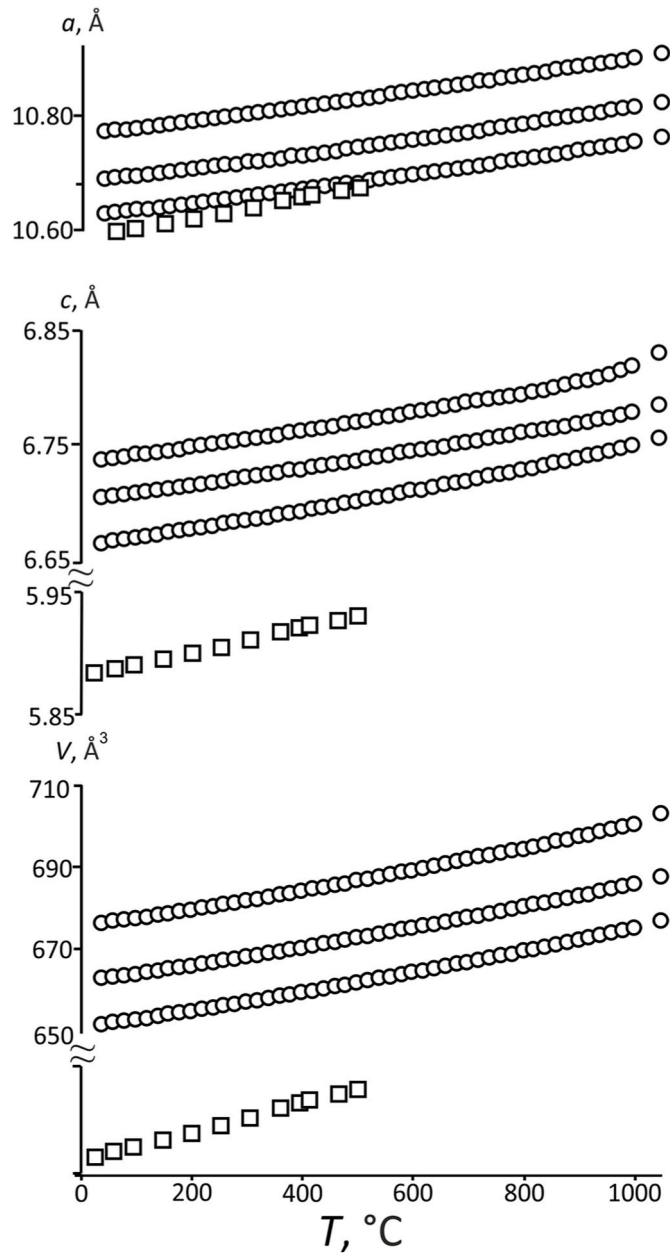
#### 3.1. DSC studies

Fig. 1 shows the DSC curves of  $\text{Sr}_2\text{MBi}(\text{YO})_3(\text{BO}_3)_4$  ( $M = \text{Ca}, \text{Sr}, \text{Ba}$ ) samples. The endothermic peaks at 1093, 1079 and 1070 °C, respectively, corresponds to decomposed temperatures (1094 °C) according to the data of previous investigation of  $\text{Sr}_3\text{Bi}(\text{YO})_3(\text{BO}_3)_4$  [8]. The

**Table 3**

Second-harmonic generation (SHG) intensity in SiO<sub>2</sub>-units from powders of Sr<sub>2</sub>MBi(REEO)<sub>3</sub>(BO<sub>3</sub>)<sub>4</sub> with M = Ca, Sr, Ba; REE = Y, Eu<sup>3+</sup>.

Composition	Sr <sub>2</sub> CaBi (YO) <sub>3</sub> (BO <sub>3</sub> ) <sub>4</sub>	Sr <sub>3</sub> Bi (YO) <sub>3</sub> (BO <sub>3</sub> ) <sub>4</sub>	Sr <sub>2</sub> BaBi (YO) <sub>3</sub> (BO <sub>3</sub> ) <sub>4</sub>	Sr <sub>2</sub> BaBi (EuO) <sub>3</sub> (BO <sub>3</sub> ) <sub>4</sub>
SHG intensity, SiO <sub>2</sub> -units	33	18	30	13



**Fig. 4.** Temperature dependencies of unit-cell parameters of the Sr<sub>2</sub>MBi(YO)<sub>3</sub>(BO<sub>3</sub>)<sub>4</sub> (M = Ca, Sr, Ba) (circles) and the gaufeyroyite Ca<sub>4</sub>(MnO)<sub>3</sub>(BO<sub>3</sub>)<sub>3</sub>(CO<sub>3</sub>) (squares).

decomposition of these borates occurs with crystallization of the Sr<sub>3</sub>Y<sub>2</sub>(BO<sub>3</sub>)<sub>4</sub> compound or (Ca, Sr)Y<sub>2</sub>(BO<sub>3</sub>)<sub>4</sub> and (Sr, Ba)Y<sub>2</sub>(BO<sub>3</sub>)<sub>4</sub> solid solutions.

**Table 4**

Thermal expansion coefficients  $\alpha$  ( $\times 10^6$  °C<sup>-1</sup>) of Sr<sub>2</sub>MBi(YO)<sub>3</sub>(BO<sub>3</sub>)<sub>4</sub> (M = Ca, Sr, Ba) and gaufeyroyite at different temperatures.

M	$\alpha_a$	$\alpha_c$	$\alpha_v$
25 °C			
Ca	9.81(6)	10.2(1)	30.0(2)
Sr	9.96(4)	9.1(1)	29.0(2)
Ba	10.45(9)	7.8(4)	28.7(4)
gaufeyroyite	14.2(9)	16.3(8)	45(2)
500 °C			
Ca	11.99(1)	12.89(3)	36.87(5)
Sr	12.16(1)	11.27(4)	35.58(5)
Ba	12.34(2)	11.83(1)	36.5(1)
gaufeyroyite	17(1)	18(1)	51(3)
1000 °C			
Ca	14.14(5)	15.7(1)	44.0(2)
Sr	14.43(4)	13.5(1)	42.4(2)
Ba	14.29(8)	16.0(4)	44.5(4)

### 3.2. Crystal structure

These Sr<sub>2</sub>MBi(YO)<sub>3</sub>(BO<sub>4</sub>)<sub>4</sub> (M = Ca, Sr, Ba) borates crystallize in gaufeyroyite structure-type in P6<sub>3</sub> space group (Table 1). The crystal structures of three borates (M = Ca, Sr, Ba) were solved and refined in P6<sub>3</sub> space group to the R<sub>1</sub> = 4, 6 and 2%, respectively. There are 10 non-equivalent atoms in the asymmetric unit. Only Bi and B(1) atoms are located in the special sites, and other atoms occupy the general sites (Table S1). The Y atom is coordinated by seven O atoms to form a pentagonal bipyramid. These YO<sub>7</sub> polyhedra share edges to form a chain or column along the c direction. The Y–O bond lengths vary from 2.24 to 2.53 Å for M = Ca, 2.27 to 2.42 Å for M = Sr, 2.15 to 2.50 Å in for M = Ba. The chains are connected by B(2)O<sub>3</sub> groups to construct a 3D-framework with two kinds of channels along the c direction. The smaller channel is filled by Bi<sup>3+</sup> cations and the larger channel is occupied by Sr atoms and B(1)O<sub>3</sub> triangles (Fig. 2).

The Ca→Sr→Ba substitutions in the Sr1 site result in an increase in a and c parameters (Table 1) due to ionic radius of [8]Ba (1.56 Å) is larger than ionic radius of [8]Ca (1.26 Å). The relative increase in a and c parameters, i.e.  $\Delta a/a$  and  $\Delta c/c$ , is about 1.5%. Upon those substitutions the average bond lengths in the Sr1O<sub>8</sub>, Bi1O<sub>6</sub> polyhedra and in the oxo-centered OM<sub>4</sub> tetrahedra increase slightly. The <Sr1–O> bond length varies from 2.59 Å to 2.66 Å, <Bi1–O> – from 2.51 Å to 2.56 Å and <O<sub>ex</sub>–M> – from 2.33 Å to 2.36 Å while the <Y1–O> bond length in Y1O<sub>7</sub> polyhedra is remains almost constant 2.35–2.36 Å (Table 2).

The Y→Eu substitution in the Sr<sub>2</sub>BaBi(EuO)<sub>3</sub>(BO<sub>3</sub>)<sub>4</sub> leads to an increase in the a parameter by approximately 0.1 Å, while the c parameter practically does not change. The unit cell parameters are: a = 10.919 (5), c = 6.752 (4) Å, V = 697.2 (6) Å<sup>3</sup> for Sr<sub>2</sub>BaBi(EuO)<sub>3</sub>(BO<sub>3</sub>)<sub>4</sub>, and a = 10.78028 (8), c = 6.74379 (6) Å, V = 678.73(1) Å<sup>3</sup> for Sr<sub>2</sub>BaBi(YO)<sub>3</sub>(BO<sub>4</sub>)<sub>4</sub>. Since the REEO<sub>7</sub> polyhedra increase with Y→Eu substitution and the parameter c practically does not increase, the chain consisting of edge-sharing EuO<sub>7</sub> polyhedra will be distorted.

There are O(5) oxygen atoms not bonded to boron. Hence, this crystal structure can be described in terms of oxy-centered polyhedra (Fig. 3). Additional oxygen atoms have [OSrBiY<sub>2</sub>] tetrahedral coordination and form oxy-centered framework [O<sub>6</sub>Sr<sub>6</sub>Bi<sub>2</sub>Y<sub>6</sub>] according to the [27]. The framework consists on pinwheels O<sub>3</sub>BiY<sub>6</sub>Sr<sub>3</sub> which are linked by vertices. The bond-valence calculations were performed using empirical parameters taken from Refs. [28,29] for additional oxygen atoms. The results are presented in Table 2. It is seen that Bi–O(5) bond is the shortest (2.07 Å) and therefore the strongest (0.85 v.u.) in the BiO<sub>6</sub> polyhedra.

There is some disordering of cations in the crystal structure. In particular, in Sr<sub>2</sub>CaBi(YO)<sub>3</sub>(BO<sub>3</sub>)<sub>4</sub>, the Sr site is partially occupied by the Ca atoms, and in Sr<sub>2</sub>BaBi(YO)<sub>3</sub>(BO<sub>3</sub>)<sub>4</sub> the Sr site is partially occupied by Ba atoms.

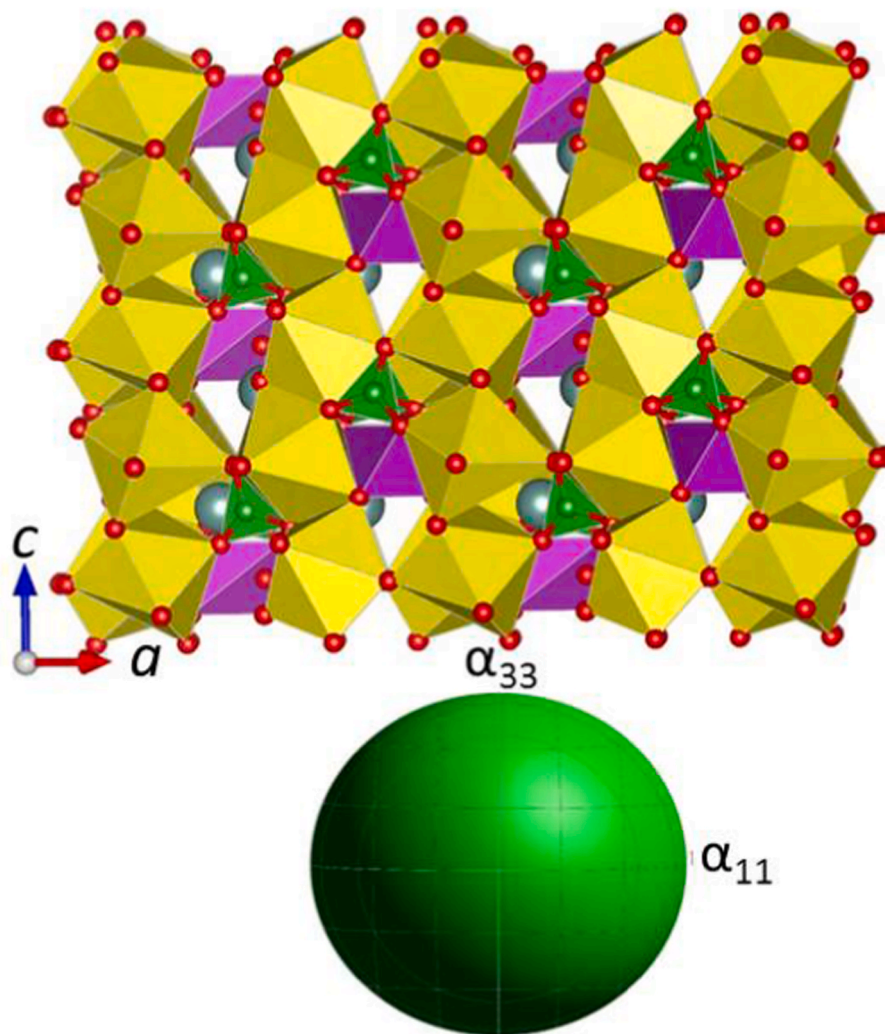


Fig. 5. The comparison of the  $\text{Sr}_3\text{Bi}(\text{YO})_3(\text{BO}_3)_4$  crystal structure and the figure of thermal expansion tensor.

### 3.3. NLO properties

Strong SHG response is observed for  $\text{Sr}_2\text{MBi}(\text{REEO})_3(\text{BO}_3)_4$  ( $M = \text{Ca}, \text{Sr}, \text{Ba}$ ;  $\text{REE} = \text{Y}, \text{Eu}^{3+}$ ) in accordance with data in Table 3. The SHG intensity is practically doubled when strontium atoms are partially replaced by calcium or barium. In comparison to  $\text{Sr}_3\text{Bi}(\text{YO})_3(\text{BO}_3)_4$  SHG output decreases when Y is replaced with Eu.  $\text{Sr}_3\text{Bi}(\text{YO})_3(\text{BO}_3)_4$  exhibits phase matching ability according to Ref. [8]. A similar values of the optical nonlinearity of all substances in Table 3 allow us to extend this property to all other listed there substances.

The analysis of the crystal structures of the compounds revealed several factors influencing on the nonlinear optical properties. Firstly, according to the anion group theory [4], it concerns the arrangement of  $\text{BO}_3$  groups. In the gaufreyite-type compounds, isolated  $\text{BO}_3$  triangles are located in the  $ac$  and approximately  $ab$  planes, so the conjugated  $\pi$ -bonding of the  $\text{BO}_3$  groups may give contributions to SHG coefficients. Secondly, the SHG activity usually is larger in substances containing ions with high electronic polarizability, the  $\text{Bi}^{3+}$ -cation being a good example due to its stereoactive lone pair of electrons. Ionic radius of alkaline-earth cations also impacts on optical nonlinearity because of their influencing on electric interactions between all ions in a crystal. According to Refs. [17,30] both electronic polarizability and ionic radii of relevant cations are changing as  $\text{Ba} > \text{Sr} > \text{Ca}$ . The positive effect of large cations is associated with an increase in the size of their polyhedra, which provides large displacements of cations from the sites. This leads

to an increase in the electric polarization of the crystal and an increase of optical nonlinearity.

Growth of second harmonic intensity at the replacement of  $\text{Sr}^{2+}$  cations with  $\text{Ca}^{2+}$  and  $\text{Ba}^{2+}$  cations may be caused by the increasing of distortion index of  $\text{BiO}_6$  polyhedra.  $\text{SrO}_8$  and  $\text{BiO}_6$  polyhedra share vertices. Partially  $\text{Ca} \rightarrow \text{Sr} \rightarrow \text{Ba}$  replacement increased Bi–O5 bonds (2.02, 2.07, 2.09 Å) respectively. Therefore, the distortion index introduced by Baur [31] of  $\text{BiO}_6$  increased from 0.177 ( $M = \text{Sr}$ ) to 0.193 ( $M = \text{Ca}, \text{Ba}$ ).

An important factor probably affecting nonlinear optical properties of the borates under consideration is an existence of additional oxygen atom  $\text{O}_{\text{ex}}$ , which is not bonded to boron. Due to this additional oxygen, the bonds within the  $\text{BiO}_6$  polyhedron are not equal, namely, the Bi– $\text{O}_{\text{ex}}$  ( $\text{O}(5)$ ) bonds are shorter in comparison with others. This factor is also responsible for strong electric polarization of  $\text{BiO}_6$  polyhedron and its large contribution to the SHG. To the best of our knowledge, this question has not yet been considered in relation to compounds of the gaufreyite-type. So, the revealed structural peculiarity for the first time gives visual explanation for the origin of optical nonlinearity in Bi-containing borates in gaufreyite-type family. The highest SHG intensity of  $\text{Sr}_2\text{CaBi}(\text{YO})_3(\text{BO}_3)_4$  relative to other compounds allows us to conclude that this factor plays a leading role in the SHG.

### 3.4. Thermal expansion

We investigated the thermal expansion of the

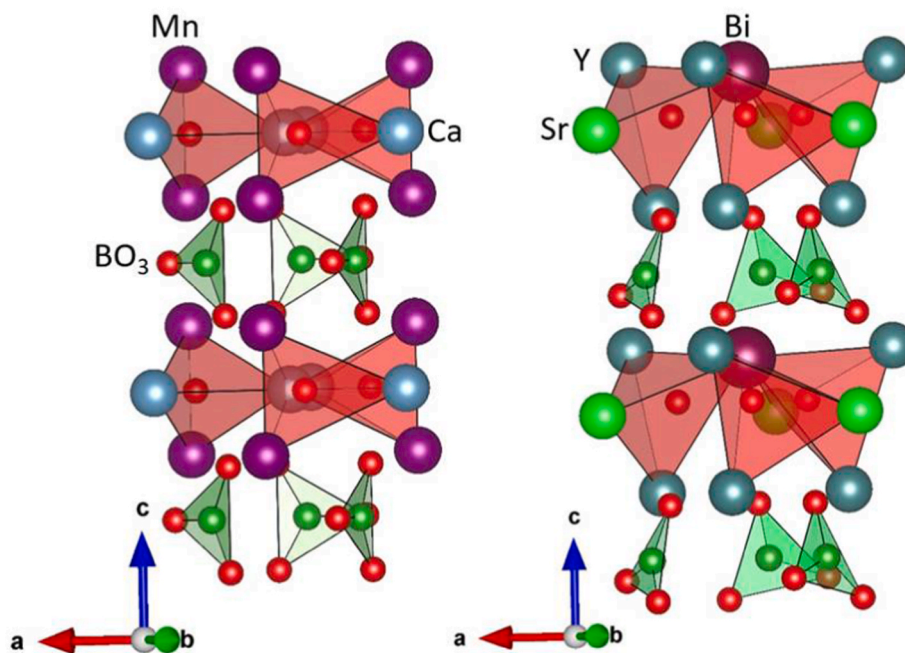


Fig. 6. Structural fragments  $O_3Mn_6Ca_4$  and  $O_3BiY_6Sr_3$  with  $BO_3$  triangles in  $Ca_4Mn_3O_3(BO_3)_3(CO_3)$  (left) and  $Sr_3Bi(YO)_3(BO_3)_4$  (right).

$Ca_4(MnO)_3(BO_3)_3(CO_3)$  gaufreyite (carbonato-borate) and the family of  $Sr_2MBi(YO)_3(BO_3)_4$  borates,  $M = Ca, Sr, Ba$ , to determine the influence of a residual charge of anion per a polyhedron as well as atomic groups arrangement on the strength properties such as thermal expansion. The volume thermal expansion of isotypical compounds with different chemical composition primarily depends on the residual charge of the anionic groups per a polyhedron [32]. If the residual charge of anion groups per a polyhedron is less the thermal expansion is greater. For example, residual charge of isolated  $[TO_3]$  radicals decreases from  $-3$  for  $[BO_3]^{3-}$  to  $-2$  for  $[CO_3]^{2-}$  and  $-1$  for  $[NO_3]^-$ . Hence, the thermal expansion of nitrates has to be maximal in comparison to carbonates and borates. This trend is demonstrated by borates, carbonates, and nitrates of a calcite-like structure [5]. For the isotypical compounds with the same anionic groups, the volume thermal expansion depends on the ionic radii and the charge of the cations [33]. The degree of anisotropy of thermal expansion is determined by the arrangement of rigid atomic groups [33].

The thermal expansion coefficients for  $Ca_4(MnO)_3(BO_3)_3(CO_3)$  gaufreyite were calculated using the high temperature single crystal X-ray diffraction data in the temperature range of 25–500 °C from Ref. [16]. The thermal evolution of the unit cell parameters for carbonato-borate (gaufreyite) and  $Sr_2MBi(YO)_3(BO_3)_4$  ( $M = Ca, Sr, Ba$ ) borates shows that the character of thermal expansion of these compounds is practically isotropic (Fig. 4). The temperature dependencies of unit cell parameters were approximated by second order polynomial function (Table S3). Thermal expansion coefficients are given in Table 4. There are no polymorphic transitions in the investigated temperature range; the decomposition of these compounds occurs with crystallization of the  $Sr_3Y_2(BO_3)_4$  compound above 1100 °C. Fig. 5 shows the comparison of the  $Sr_3Bi(YO)_3(BO_3)_4$  crystal structure and the figure of thermal expansion tensor.

There are two types of the rigid structural units with strong chemical bonds in the crystal structure of  $Ca_4(MnO)_3(BO_3)_3(CO_3)$  gaufreyite:  $[CO_3]$  and  $[BO_3]$  triangular groups. The residual charge of the  $[CO_3]^{2-}$  anionic group is lower than the  $[BO_3]^{3-}$  group, so the volume expansion of the carbonato-borate will be greater than that of borates (Table 4).

The  $[CO_3]$  and  $[BO_3]$  triangular groups located in  $ab$  and  $ac$  planes provide almost isotropic character of thermal expansion because of their perpendicular orientation to each other. Therefore, the thermal

expansion in the direction perpendicular to the plane of  $[CO_3]$  triangles ( $ab$ ) is insignificantly higher than the thermal expansion in the direction perpendicular to the  $BO_3$  triangles.

In the  $Sr_2MBi(YO)_3(BO_3)_4$  ( $M = Ca, Sr, Ba$ ) borates, the  $[CO_3]$  groups in the channels are substituted by  $[BO_3]$  triangular groups, and Ca atoms in special sites are substituted by Bi atoms to compensate the charge balance. Due to the substitution of  $CO_3$  groups for the  $BO_3$  groups, the relation of  $\alpha_a$  and  $\alpha_c$  thermal expansion coefficients is slightly changed and now the thermal expansion in  $a$  direction is higher.

Let us consider the assumed crystal-chemical reason for this feature. The possible reason for the difference in the thermal expansion of gaufreyite and  $Sr_2MBi(YO)_3(BO_3)_4$  ( $M = Ca, Sr, Ba$ ) borates is structural distortions. These distortions are caused by the presence of stereoactive lone electron pair of  $Bi^{3+}$ . In the crystal structure of gaufreyite  $Ca_4(MnO)_3(BO_3)_3(CO_3)$ , three oxy-centered tetrahedra are connected by one Ca atom and  $BO_3$  triangles are in the  $ac$  plane (Fig. 6a). In the crystal structure of the borates, the fragment changes. When Bi atoms substitute Ca atoms in this site, the stereoactive lone electron pairs repulse  $BO_3$  triangles, and their orientation is changed (Fig. 6b). Thus,  $BO_3$  triangles are not strictly parallel to  $[001]$  in  $Sr_2MBi(YO)_3(BO_3)_4$  ( $M = Ca, Sr, Ba$ ) borates. Therefore, thermal expansion coefficients are lowered. So, the structural distortions can influence on the thermal expansion coefficients. Moreover, these distortions of cation and anion-centered frameworks lead to a change in the space group and the appearance of nonlinear optical properties.

### 3.5. Theoretical studies

The band structure of  $Sr_3Bi(YO)_3(BO_3)_4$  is presented in Fig. 7a. For convenience, the Fermi level was shifted to 0 eV when discussing the electronic structures. The top of the valence bands (VBs) is located at  $\Gamma$  point, and the bottom of the conduction bands is located at the point between  $\Gamma$  and A points. So it has an indirect band gap of 2.40 eV. The total and partial density of states (DOS and PDOS, respectively) is presented in Fig. 7b. The VBs ranging between  $-22$  and  $-16$  eV are composed of B-2s2p, and O-2s, with small amount of O-2p and Bi-6s6p orbitals, where high orbital hybridization is on the O and B orbitals. The VBs ranging from  $-9$  to  $E_f$  are formed by Bi-6s6p, Y-4d, B-2s2p, and O-2s2p, with high orbital hybridization on the O and Bi/Y/B orbitals;

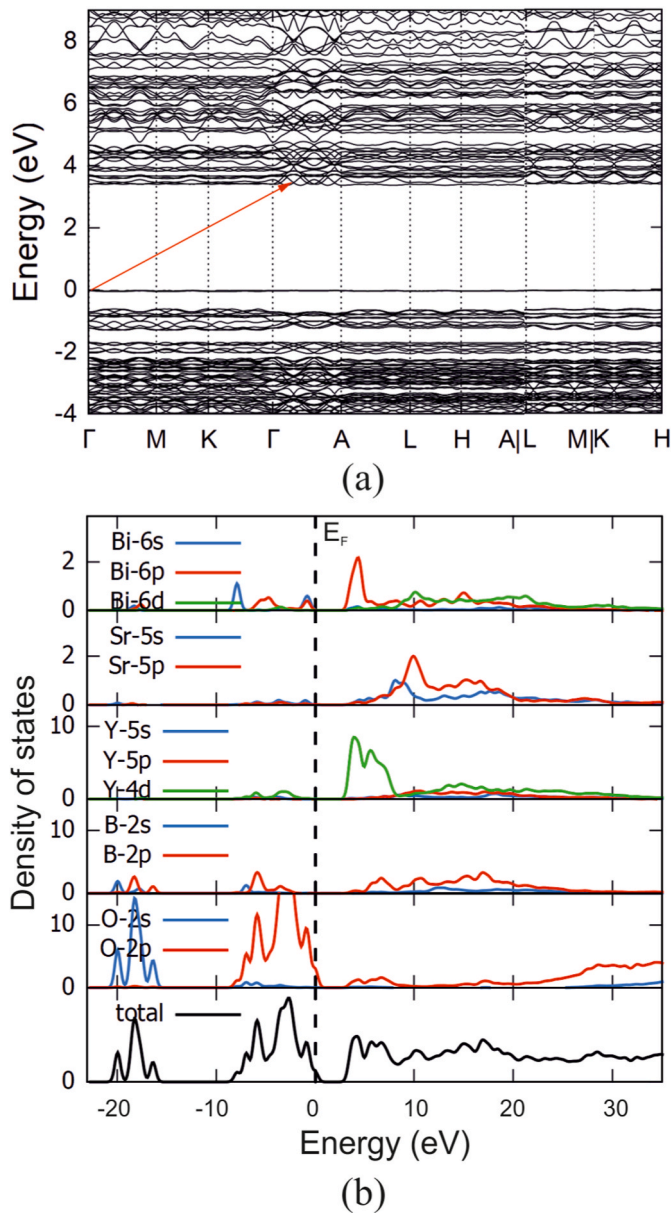


Fig. 7. The band structure (a), total and partial density of states (b) of  $\text{Sr}_3\text{Bi}(\text{YO})_3(\text{BO}_3)_4$  (the Fermi level is set at 0 eV).

therefore there is strong covalent bonding between the Bi/Y/B and O atoms. Bi-6p6d, Sr-5s5p, Y-5s5p4d, B-2p, and O-2p with small amount of O-2s, B-2s and Bi-6s orbitals make up the conduction bands (CBs).

The band structure of  $\text{Sr}_2\text{CaBi}(\text{YO})_3(\text{BO}_3)_4$  is presented in Fig. 8a. The top of the valence bands (VBs) is located at  $\Gamma$  point, and the bottom of the conduction bands is located at the point between  $\Gamma$  and M points. So it has an indirect band gap of 2.45 eV, close to that of  $\text{Sr}_3\text{Bi}(\text{YO})_3(\text{BO}_3)_4$  value due to the both compounds are isotypical. The total and partial density of states (DOS and PDOS, respectively) is presented in Fig. 8b. The VBs ranging between  $-21$  and  $-16$  eV are composed of B-2s2p, and O-2s2p (unlike O-2s only for  $\text{Sr}_3\text{Bi}(\text{YO})_3(\text{BO}_3)_4$ ), with small amount of Bi-6s6p and Sr-5s orbitals, where high orbital hybridization is on the O and B orbitals. The VBs ranging from  $-9$  to  $E_f$  are formed by Bi-6s6p, Sr-5s, Y-5s4d, B-2s2p, and O-2s2p, with orbital hybridization on the O and Bi/Sr/Y/B orbitals. Bi-6p6d, Sr-5s5p, Ca-4s4p, Y-5s5p4d, B-2p, and O-2p with small amount of O-2s, B-2s and Bi-6s orbitals make up the conduction bands (CBs).

We calculate the electron-density distribution using the density

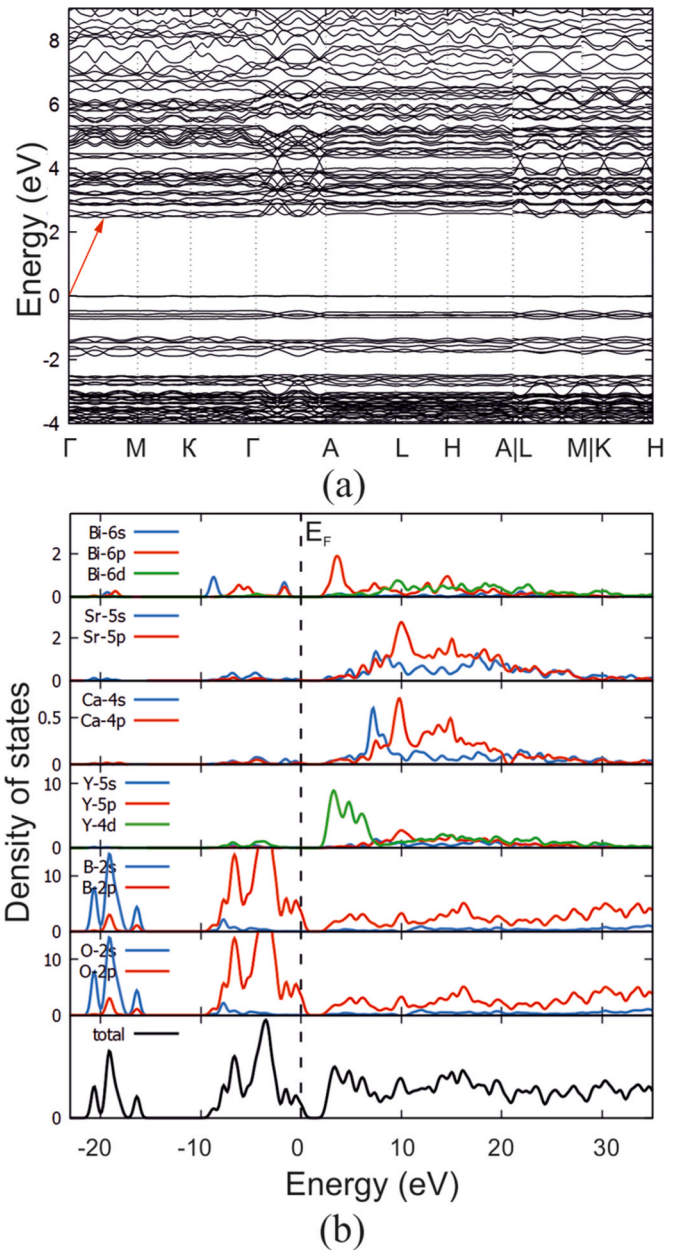


Fig. 8. The band structure (a), total and partial density of states (b) of  $\text{Sr}_2\text{CaBi}(\text{YO})_3(\text{BO}_3)_4$  (the Fermi level is set at 0 eV).

functional theory (DFT). Fig. 3b shows the ELF = 0.88 isosurface, which clearly identifies the presence of a stereoactive electron pair of  $\text{Bi}^{3+}$  atoms.

#### 4. Conclusion

Novel non-centrosymmetric borates  $\text{Sr}_3\text{Bi}(\text{YO})_3(\text{BO}_3)_4$ ,  $\text{Sr}_2\text{CaBi}(\text{YO})_3(\text{BO}_3)_4$  and  $\text{Sr}_2\text{BaBi}(\text{YO})_3(\text{BO}_3)_4$  with large second harmonic generation responses were synthesized by solid state reactions and characterized by powder and single crystal X-ray diffraction in the wide range of temperatures, as well as by thermal analysis. The SHG intensity is practically doubled when strontium atoms are partially replaced by calcium or barium ones.

Several factors affecting the nonlinear optical properties may be explained:  $\text{BO}_3$  groups arrangement, polarizability and ionic radii of Ca, Sr and Ba cations,  $\text{Bi}^{3+}\text{O}_6$  asymmetric coordination due to presence of additional oxygen in the coordination of  $\text{Bi}^{3+}$  cation. The effect of the

last factor on the structural nature of the nonlinear optical properties of borates of the  $\text{Sr}_3\text{Bi}(\text{YO})_3(\text{BO}_3)_4$  family was investigated for the first time.

The thermal evolution of the unit cell parameters for carbonato-borate (gaudfroyite) and  $\text{Sr}_2\text{M}(\text{YO})_3(\text{BO}_3)_4$  ( $M = \text{Ca}, \text{Sr}, \text{Ba}$ ) borates shows that the character of thermal expansion of these compounds is almost isotropic due to the orientation of  $\text{BO}_3$  ( $\text{CO}_3$ ) triangles both in the  $ab$  and in the  $ac$  planes. The structural reason of the difference in thermal expansion between gaudfroyite and  $\text{Sr}_3\text{Bi}(\text{YO})_3(\text{BO}_3)_4$  family may be the substitution of  $\text{CO}_3$  groups for the  $\text{BO}_3$  groups and structural distortions due to stereoactive lone electron pair.

### CRedit (contribution roles taxonomy)

Rimma S. Bubnova – Conceptualization, Supervision Writing – Review & Editing; Andrey P. Shablinskii – Conceptualization, Formal Analysis, Visualization, Investigation, Writing – Original Draft Preparation, Writing – Review & Editing, Supervision; Sergey Yu. Stefanovich – Investigation, Writing – Review & Editing; Maxim Yu. Arsent'ev – Investigation, Visualization; Maria G. Krzhizhanovskaya – Investigation, Writing – Review & Editing; Bogdan I. Lazoryak – Investigation; Valery L. Ugol'kov – Investigation; Stanislav K. Filatov – Conceptualization, Supervision.

### Declaration of competing interest

The authors declare that they have no known competing financial interests or personal relationships that could have appeared to influence the work reported in this paper.

### Acknowledgement

This work was financially supported by the Russian Science Foundation (RSF) [grant no. 22-13-00317] and the Ministry of Science and Higher Education of the Russian Federation within the scientific tasks of the Institute of Silicate Chemistry (Russian Academy of Sciences) [project number 0081-2022-0002] scientific task. Technical support by the SPbSU X-ray Diffraction Centre is gratefully acknowledged.

### Appendix A. Supplementary data

Supplementary data to this article can be found online at <https://doi.org/10.1016/j.ceramint.2023.01.091>.

### References

- P.F. Gong, X.M. Liu, L. Kang, Z.S. Lin, Inorganic planar  $\pi$ -conjugated groups in nonlinear optical crystals: review and outlook, *Inorg. Chem. Front.* 7 (2020) 839–852, <https://doi.org/10.1039/C9QI01589B>.
- Y. Shen, S. Zhao, J. Luo, The role of cations in second-order nonlinear optical materials based on  $\pi$ -conjugated  $[\text{BO}_3]^{3-}$  groups, *Coord. Chem. Rev.* 366 (2018) 1–28, <https://doi.org/10.1016/j.ccr.2018.03.012>.
- M. Mutailipu, K.R. Poeppelmeier, S. Pan Borates, A rich source for optical materials, *Chem. Rev.* 121 (2021) 1130–1202, <https://doi.org/10.1021/acs.chemrev.0c00796>.
- C. Chen, T. Sasaki, R. Li, Y. Wu, Z. Lin, Y. Mori, Z. Hu, J. Wang, S. Uda, M. Yoshimura, Y. Kaneda, *Nonlinear Optical Borate Crystals*, Wiley-VCH Verlag GmbH & Co. KGaA, Weinheim, Germany, 2012.
- R.S. Bubnova, S.K. Filatov, Self-assembly and high anisotropy thermal expansion of compounds consisting of  $\text{TO}_3$  triangular radicals, *Struct. Chem.* 27 (2016) 1647–1662, <https://doi.org/10.1007/s11224-016-0807-9>.
- H. Hellwig, J. Liebertz, L. Bohaty, Exceptional large nonlinear optical coefficients in the monoclinic bismuth borate  $\text{BiB}_3\text{O}_6$  (BIBO), *Solid State Commun.* 109 (1998) 249–251, [https://doi.org/10.1016/S0038-1098\(98\)00538-9](https://doi.org/10.1016/S0038-1098(98)00538-9).
- J. Zhao, D. Mei, W. Wang, Y. Wu, D. Xu, Recent advances in nonlinear optical rare earth structures, *J. Rare Earths* 39 (2021) 1455–1466, <https://doi.org/10.1016/j.jre.2021.07.005>.
- J. Gao, S. Li,  $\text{BiSr}_3(\text{YO})_3(\text{BO}_3)_4$ : a new gaudfroyite-type rare-earth borate with moderate SHG response, *Inorg. Chem.* 51 (2012) 420–424, <https://doi.org/10.1021/ic201858x>.
- G. Jouravsky, F. Permingeat, La gaudfroyite, une nouvelle espèce minérale, *Bull. Soc. Fr. Mineral. Cristallogr.* 87 (1964) 216–229.
- O.V. Yakubovich, M.A. Simonov, N.V. Belov, Structure refinement for gaudfroyite, *Sov. Phys. Crystallogr.* 20 (1975) 87–88.
- X. Chen, H. Yin, X. Chang, H. Zhang, W. Xiao, Synthesis, crystal structure, spectrum properties, and electronic structure of a novel non-centrosymmetric borate,  $\text{BiCd}_3(\text{AlO})_3(\text{BO}_3)_4$ , *J. Solid State Chem.* 183 (2010) 2910–2916, <https://doi.org/10.1016/j.jssc.2010.09.030>.
- R.K. Li, C. Greaves,  $\text{YCa}_3(\text{MnO})_3(\text{BO}_3)_4$ : a manganese borate containing ferromagnetic chains on a kagome lattice, *Phys. Rev. Cond. Matt.* 68 (2003), 172403, <https://doi.org/10.1103/PhysRevB.68.172403>.
- Y. Yu, Q.S. Wu, R.K. Li, Structure of two new borates  $\text{YCa}_3(\text{AlO})_3(\text{BO}_3)_4$  and  $\text{YCa}_3(\text{GaO})_3(\text{BO}_3)_4$ , *J. Solid State Chem.* 179 (2006) 429–432, <https://doi.org/10.1016/j.jssc.2005.11.004>.
- W. Miller, M. Christensen, A. Khan, N. Sharma, R.B. Macquart, M. Avdeev, G. J. McIntyre, R.O. Piltz, C.D. Ling,  $\text{YCa}_3(\text{VO})_3(\text{BO}_3)_4$ : a kagomé compound based on vanadium(III) with a highly frustrated ground state, *Chem. Mater.* 23 (2011) 1315–1322, <https://doi.org/10.1021/cm1034003>.
- C. Hoffmann, T. Armbruster, M. Kunz, Structure refinement of (001) disordered gaudfroyite  $\text{Ca}_4(\text{Mn}^{3+})_3(\text{BO}_3)_3(\text{CO}_3)_2$ : jahn-Teller-distortion in edge-sharing chains of  $\text{Mn}^{3+}\text{O}_6$  octahedra, *Eur. J. Mineral.* 9 (1997) 7–19, <https://doi.org/10.1127/ejm/9/1/0007>.
- S.M. Antao, I. Hassan, Gaudfroyite,  $\text{Ca}_8\text{Mn}^{(3+)}_6(\text{BO}_3)_6(\text{CO}_3)_2\text{O}_6$ : high-temperature crystal structure, *Can. Mineral.* 46 (2008) 183–193, <https://doi.org/10.3749/canmin.46.1.183>.
- P. Schwerdtfeger, J.K. Nagle, Table of static dipole polarizabilities of the neutral elements in the periodic table, *Mol. Phys.* 117 (2018) 1200–1225, 2019.
- H. Yu, Z. Pan, H. Zhang, J. Wang, Recent advances in self-frequency-doubling crystals, *J. Mater. Chem.* 2 (2016) 55–65, <https://doi.org/10.1016/j.jmat.2015.12.001>.
- Bruker AXS, Topas 5.0: General Profile and Structure Analysis Software for Powder Diffraction Data, Karlsruhe, Germany, 2014.
- Jana2006 V. Petricek, M. Dusek, L. Palatinus, *The Crystallographic Computing System*, Institute of Physics, Academy of Sciences of the Czech Republic, Prague, 2006.
- R.S. Bubnova, V.A. Firsova, S.N. Volkov, S.K. Filatov RietveldToTensor, Program for processing powder X-ray diffraction data under variable conditions, *Glass Phys. Chem.* 44 (2018) 33–40, <https://doi.org/10.1134/S1087659618010054>.
- S.K. Kurtz, T.T. Perry, A powder technique for the evaluation of nonlinear optical materials, *J. Appl. Phys.* 39 (1968) 3798, <https://doi.org/10.1063/1.1656857>.
- J.M. Soler, E. Artacho, J.D. Gale, A. García, J. Junquera, P. Ordejón, D. Sánchez-Portal, The SIESTA method for ab initio order-N materials simulation, *J. Phys. Condens. Matter* 14 (2002) 2745–2779, <https://doi.org/10.1088/0953-8984/14/11/302>.
- J.P. Perdew, K. Burke, M. Ernzerhof, Generalized gradient approximation made simple, *Phys. Rev. Lett.* 77 (1996) 3865–3868, <https://doi.org/10.1103/PhysRevLett.77.3865>.
- N. Troullier, J.L. Martins, Efficient pseudopotentials for plane-wave calculations, *Phys. Rev. B* 43 (1991) 1993–2006, <https://doi.org/10.1103/PhysRevB.43.1993>.
- P. Giannozzi, S. Baroni, N. Bonini, M. Calandra, R. Car, C. Cavazzoni, D. Ceresoli, G.L. Chiarotti, M. Cococcioni, I. Dabo, A.D. Cprso, S. Gironcoli, S. Fabris, G. Fratesi, R. Gebauer, U. Gerstmann, C. Gougousis, A. Kokalj, M. Lazzeri, L. Martin-Samos, N. Marzari, F. Mauri, R. Mazzarello, S. Paolini, A. Pasquarello, L. Paulatto, C. Sbraccia, S. Scandolo, G. Sclauzero, A.P. Seitsonen, A. Smogunov, P. Umari, R. M. Wentzcovitch, Quantum ESPRESSO: a modular and open-source software project for quantum simulations of materials, *J. Phys. Condens. Matter* 21 (2009), 395502, <https://doi.org/10.1088/0953-8984/21/39/395502>.
- S.V. Krivovichev, S.K. Filatov, *Crystal Chemistry of Minerals and Inorganic Compounds with Complexes of Anion-Centered Tetrahedra*, St. Petersburg University Press, St. Petersburg, 2001.
- I.D. Brown, D. Altermatt, Bond-valence parameters obtained from a systematic analysis of the inorganic crystal structure Database, *Acta Crystallogr.* B41 (1985) 244–247, <https://doi.org/10.1107/S0108768185002063>.
- S.V. Krivovichev, Derivation of bond-valence parameters for some cation-oxygen pairs on the basis of empirical relationships between  $r_0$  and  $b$ , *Z. Kristallogr.* 227 (2012) 575–579, <https://doi.org/10.1524/zkri.2012.1469>.
- R.D. Shannon, Revised effective ionic radii and systematic studies of interatomic distances in halides and chalcogenides, *Acta Crystallogr.* A32 (1976) 751–767, <https://doi.org/10.1107/S0567740874004560>.
- W.H. Baur, The geometry of polyhedral distortions. Predictive relationships for the phosphate group, *Acta Crystallogr.* B30 (1974) 1195–1215, <https://doi.org/10.1107/S0567740874004560>.
- S.K. Filatov, Negative linear thermal expansion of oblique-angle (monoclinic and triclinic) crystals as a common case, *Phys. Status Solidi* 245 (2008) 2490–2496, <https://doi.org/10.1002/psb.200880256>.
- R.S. Bubnova, S.K. Filatov, High-temperature borate crystal chemistry, *Z. Kristallogr.* 228 (2013) 395–428, <https://doi.org/10.1524/zkri.2013.1646>.